

# Nodal superconducting gap structure in ferropnictide superconductor $\text{BaFe}_2(\text{As}_{0.7}\text{P}_{0.3})_2$

Y. Zhang,<sup>1</sup> Z. R. Ye,<sup>1</sup> Q. Q. Ge,<sup>1</sup> F. Chen,<sup>1</sup> Juan Jiang,<sup>1</sup> M. Xu,<sup>1</sup> B. P. Xie,<sup>1</sup> and D. L. Feng<sup>1,\*</sup>

<sup>1</sup>State Key Laboratory of Surface Physics, Department of Physics,  
and Advanced Materials Laboratory, Fudan University, Shanghai 200433, People's Republic of China

The superconducting gap is a pivotal character for a superconductor. While the cuprates and conventional phonon-mediated superconductors are characterized by distinct  $d$ -wave and  $s$ -wave pairing symmetry with nodal and nodeless gap distribution respectively, the superconducting gap distributions in iron-based superconductors are rather diversified. While nodeless gap distributions have been directly observed in  $\text{Ba}_{1-x}\text{K}_x\text{Fe}_2\text{As}_2$ ,  $\text{BaFe}_{2-x}\text{Co}_x\text{As}_2$ ,  $\text{K}_x\text{Fe}_{2-y}\text{Se}_2$ , and  $\text{FeTe}_{1-x}\text{Se}_x$  [1–4], the signatures of nodal superconducting gap have been reported in  $\text{LaOFeP}$ ,  $\text{LiFeP}$ ,  $\text{KFe}_2\text{As}_2$ ,  $\text{BaFe}_2(\text{As}_{1-x}\text{P}_x)_2$ ,  $\text{BaFe}_{2-x}\text{Ru}_x\text{As}_2$  and  $\text{FeSe}$  [5–12]. We here report the angle resolved photoemission spectroscopy (ARPES) measurements on the superconducting gap structure of  $\text{BaFe}_2(\text{As}_{1-x}\text{P}_x)_2$  in the momentum space, and particularly, the first direct observation of a circular line node on the largest hole Fermi surface around the Z point at the Brillouin zone boundary. Our data rules out the  $d$ -wave pairing origin of the nodal gap, and unify both the nodal and nodeless gaps in iron pnictides under the  $s^\pm$  pairing symmetry.

The pairing symmetry of the Cooper pair in a superconductor is manifested in its gap structure. Particularly, nodes or nodal lines of the superconducting gap often imply unconventional (*e.g.* non- $s$ -wave) pairing symmetries. For most iron-based superconductors, there are electron Fermi surfaces at the Brillouin zone corner and hole Fermi surfaces at the center. It has been proposed that the pairing interactions between the electron and hole Fermi surfaces will induce nodeless  $s$ -wave order parameter with opposite signs on them [13–15]. While this nodeless  $s^\pm$ -wave pairing symmetry has gained increasing experimental support [16–18], nodal gap has been reported in  $\text{LaOFeP}$ ,  $\text{LiFeP}$ ,  $\text{KFe}_2\text{As}_2$ ,  $\text{BaFe}_2(\text{As}_{1-x}\text{P}_x)_2$ ,  $\text{BaFe}_{2-x}\text{Ru}_x\text{As}_2$ , and  $\text{FeSe}$  by thermal conductivity, penetration depth, nuclear magnetic resonance, and scanning tunneling spectroscopy studies [5–12]. However, no direct measurement on any of these compounds has been reported regarding the gap structure so far, and especially the location of the nodes remains unknown. Since  $\text{BaFe}_2(\text{As}_{1-x}\text{P}_x)_2$  has relatively high superconducting transition temperature  $T_c$ , it provides an opportunity for direct access of the detailed gap structure in the momentum space by angle resolved photoemission spectroscopy (ARPES).

We have conducted ARPES measurements on  $\text{BaFe}_2(\text{As}_{0.7}\text{P}_{0.3})_2$  with a  $T_c$  of 30 K (see Method section for details). As previous detailed polarization dependent studies have shown [19] and replicated here in Fig. 1a, there

are three hole like Fermi surfaces ( $\alpha$ ,  $\beta$ , and  $\gamma$ ) surrounding the central  $\Gamma$  – Z axis of the Brillouin zone, and two electron Fermi surfaces ( $\delta$  and  $\eta$ ) around the Brillouin zone corner M-A. Near  $\Gamma$ , the  $\alpha$  and  $\beta$  Fermi surfaces are coincident, and these two bands are mainly composed of Fe  $d_{xz}$  and  $d_{yz}$  orbitals near  $\Gamma$ . The  $\gamma$  band is composed of the  $d_{xy}$  orbital, and shows little  $k_z$  dispersion [19]. Compared with the Fermi surfaces of  $\text{Ba}_{0.6}\text{K}_{0.4}\text{Fe}_2\text{As}_2$  [20], the Fermi surface of the  $\alpha$  band in  $\text{BaFe}_2(\text{As}_{0.7}\text{P}_{0.3})_2$  exhibits a much larger warping away from  $\Gamma$ , so that it moves outward and becomes the outmost Fermi surface around Z [19, 21]. To examine the superconducting gap, Fig. 1b shows the symmetrized photoemission intensity in the normal and superconducting state taken along the cut #1 across  $\Gamma$ . By symmetrizing, the temperature broadening effect of the Fermi-Dirac distribution on the spectrum can be minimized. By comparing the data at two different temperatures, one could see that the spectral weight near the Fermi energy ( $E_F$ ) are suppressed in the superconducting state. More specifically, the temperature dependence of the symmetrized photoemission spectra at the Fermi crossings of the  $\alpha/\beta$  and  $\gamma$  bands are shown in Fig. 1c. In the normal state, there is a spectral weight dip near the Fermi energy. It could be due to the combined effect of fast dispersion nature of the band and limited momentum resolution, or due to the intrinsic correlation effects on the lineshape. Above  $T_c$ , such a dip does not change noticeably from 41 K to 36 K. Upon entering the superconducting state, the spectral weight near the Fermi energy is further suppressed quickly with decreasing temperature. A small superconducting coherent peak can be observed at 8 K. To remove the effects of the normal state lineshape, the 41 K data are deducted from the low temperature spectra, and it is clear that such a suppression is related to the opening of a superconducting gap. By fitting the spectra with a typical superconducting state spectral function (as exemplified in Fig. 1c and Fig. S2 in the supplementary materials), we could obtain the temperature dependence of the superconducting gap in Fig. 1d, which can be fitted well to the BCS formula (solid line). Similarly, the opening of the superconducting gap on the  $\delta$  and  $\eta$  Fermi surfaces are illustrated in Figs. 1e-1g for  $k_z = 0.54\pi$ . The extrapolated zero temperature gaps give  $2\Delta_0/k_B T_c \approx 5 \sim 6$  for  $\text{BaFe}_2(\text{As}_{0.7}\text{P}_{0.3})_2$ . The  $k_z$  is calculated and folded into the upper half of the first Brillouin zone hereafter (see supplementary materials for details). It is denoted in the unit of  $1/c'$ , where  $c'$  is the distance between two neighboring FeAs layers, which is half of the out-of-plane lattice constant  $c$ .

Recent angle dependent transport experiments [7] have suggested that the superconducting gap nodes might be located on the electron Fermi surfaces. Figure 2, together with more data in the supplementary materials, gives an extensive survey of

\*Electronic address: dlfeng@fudan.edu.cn

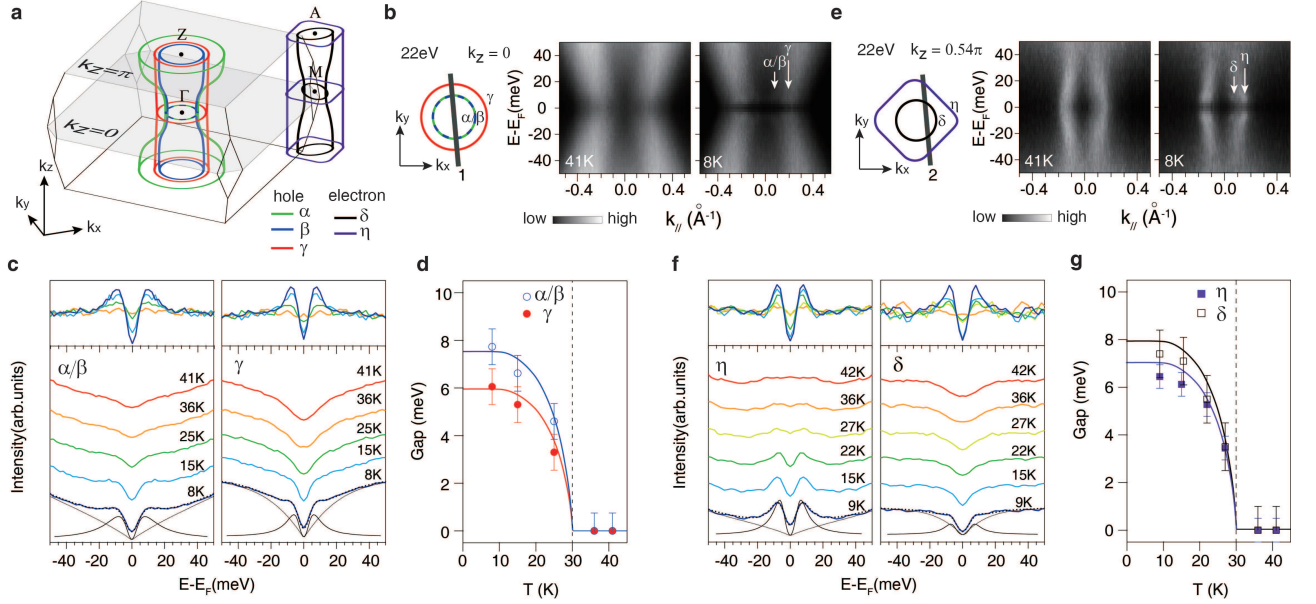


FIG. 1: **The temperature dependence of the photoemission spectra of  $\text{BaFe}_2(\text{As}_{0.7}\text{P}_{0.3})_2$ .** **a**, The three-dimensional Fermi surfaces of  $\text{BaFe}_2(\text{As}_{0.7}\text{P}_{0.3})_2$ . The two-iron unit cell are implemented here, with Fe-Fe direction as the  $k_x$  direction. The electron Fermi surfaces are only illustrated at one corner of the Brillouin zone for simplicity. **b**, The photoemission intensity taken around the zone center with 22 eV photons at 41 and 8 K. **c**, The temperature dependence of the symmetrized spectra measured at the Fermi crossings of  $\alpha/\beta$  and  $\gamma$  along the cut in **b**. The top panel are the low temperature symmetrized spectra after subtracting the 41 K one. **d**, The temperature dependence of the superconducting gaps of the  $\alpha/\beta$  and  $\gamma$  band. The gap size is estimated by fitting the symmetrized spectra as described in the supplementary materials. Two examples of the fitted curve, background, and superconducting spectral function are shown in black dashed line, dot line, and solid line respectively. **e**, **f**, and **g** are the same as **b**, **c**, and **d**, but taken around the zone corner along cut #2 with 22 eV photons. The error bars in **d** and **g** are standard deviations of the measured superconducting gaps.

gap on the electron Fermi surfaces. Figure 2a shows four typical cuts in the  $k_z = 0.5\pi$  plane, and finite gaps clearly open in all cases. The superconducting state spectra taken along the normal state  $\eta$  Fermi surface are shown in Fig. 2b for its  $k_z = 0, 0.5\pi$ , and  $\pi$  horizontal cross-sections, and in Fig. 2c for its  $k_z - k_y$  vertical cross-section. Similarly, Figs. 2d and 2e plot the spectra on the  $\delta$  Fermi surface. In addition, similar data taken in the  $k_z = 0.2\pi, 0.34\pi, 0.54\pi, 0.64\pi, 0.8\pi$  planes are shown in Fig. S4 of the supplementary materials. The superconducting gaps are finite in all cases, and the in-plane gap distribution is always isotropic. If the gap nodes were continuously located along certain vertical lines or loops on the Fermi surface as suggested [7, 22–24], they should not be missed in such an extensive search. Therefore, we could conclude that the line nodes of the gap are absent on the electron Fermi surfaces.

Phosphor doping is predicted to alter the band structure and Fermi surface topology dramatically [22, 25]. Particularly, it is predicted that the  $d_{3z^2-r^2}$ -based band would go above  $E_F$ , while the  $d_{xy}$ -based band would move down below the  $E_F$  with phosphor doping. Several theories predicted that vertical line nodes will appear in the electron Fermi surface when the  $d_{xy}$  hole Fermi surface disappears [22–24]. The fact that the  $d_{xy}$  band (*i.e.* the  $\gamma$  band) does not sink below  $E_F$ , and the absence of vertical nodes on the electron Fermi surfaces all indicate that this is not the case in  $\text{BaFe}_2(\text{As}_{1-x}\text{P}_x)_2$ .

Figure 3 gives the detailed map of superconducting gaps on

the hole Fermi surfaces. The symmetrized spectra along the  $\beta$ ,  $\gamma$ , and  $\alpha$  Fermi surfaces are shown in Figs. 3a, 3b and 3c respectively as a function of  $k_z$ . As indicated by the dashed line, the superconducting gap decreases slightly from  $k_z = 0$  to  $k_z = \pi$  for both the  $\beta$  and  $\gamma$  bands. Remarkably, the gap of  $\alpha$  exhibits a much larger variation than the other two, and it even closes near the Z point. To further highlight the nodal gap distribution, the photoemission intensity along three cuts in the  $k_z = \pi$  plane are shown in Fig. 3d, it is clear that the gap opens on the  $\beta$  and  $\gamma$  bands, but not on the  $\alpha$  band in the data taken simultaneously. Figure 3e further displays the symmetrized spectra around the three Fermi surfaces in the  $k_z = \pi$  plane. The gap exhibits a circular line node around the Z point on the  $\alpha$  Fermi surface, while the gaps on the  $\beta$  and  $\gamma$  Fermi surfaces are finite and isotropic within the experimental resolution. As a comparison, the data taken in the  $k_z = 0.38\pi$  plane shows full gap for all three Fermi surfaces (Figs. 3f-3g). Such a horizontal line node distribution immediately rules out the *d*-wave pairing symmetry, which would give four vertical line nodes in the diagonal directions like in the cuprates.

We note that our finding naturally explains the four-fold symmetry of the angle dependent thermal conductivity [7], since the Fermi velocity along the circular nodal line is four-fold symmetric. Moreover, a recent ARPES measurement with 7 eV laser on  $\text{BaFe}_2(\text{As}_{0.65}\text{P}_{0.35})_2$  has claimed a nodeless gap around Z [26]. However based on our extensive photon energy dependence study, 7 eV photon actually measures

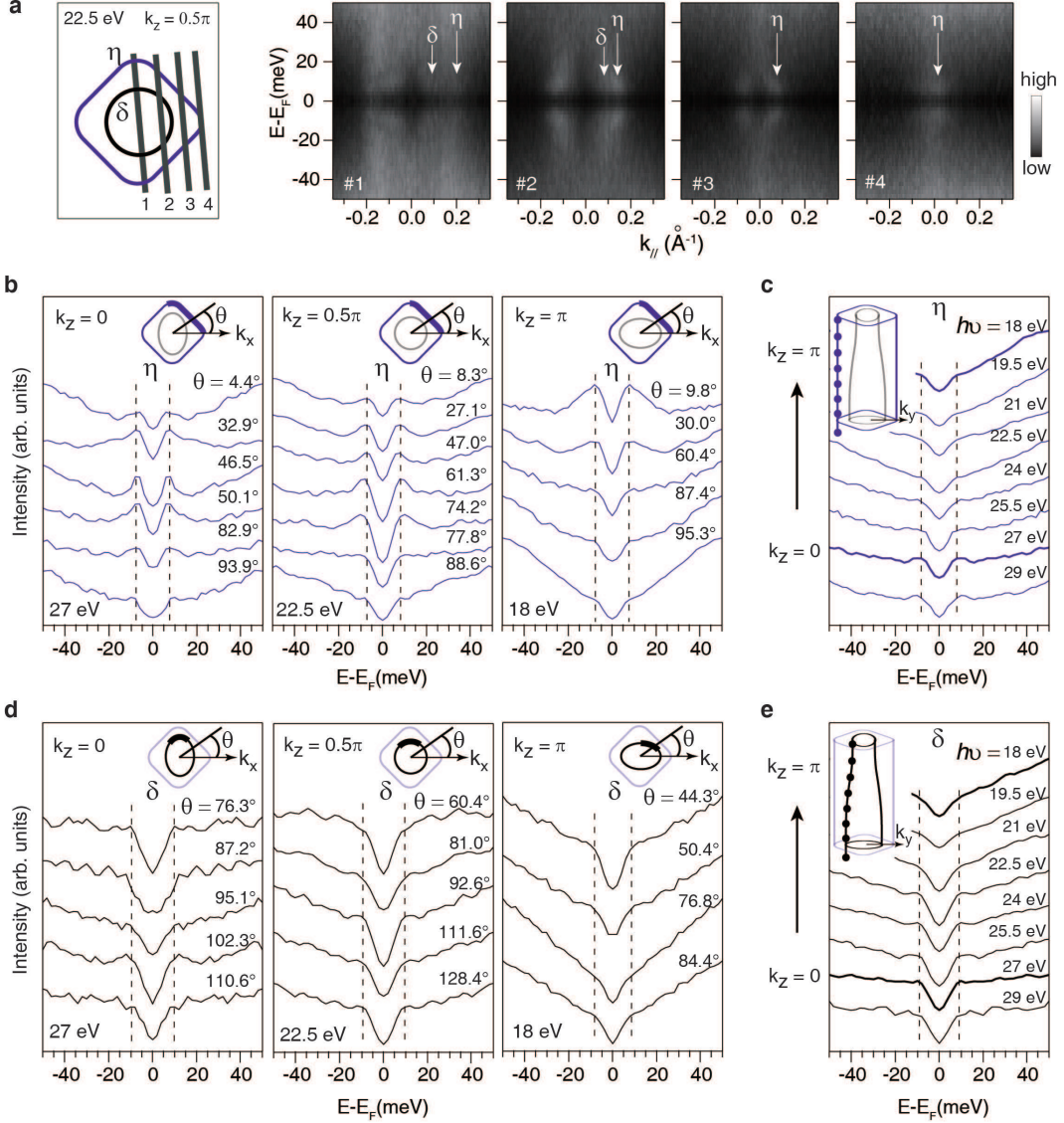


FIG. 2: **The superconducting gap distribution on the electron Fermi surfaces of  $\text{BaFe}_2(\text{As}_{0.7}\text{P}_{0.3})_2$ .** **a**, The photoemission intensities taken along different momentum cuts near the zone corner with 22.5 eV photons. **b**, Angular-dependent symmetrized spectra of the  $\eta$  electron Fermi surface measured at three typical  $k_z$ 's with 27, 22.5 and 18 eV photons. **c**,  $k_z$ -dependence of the symmetrized spectra measured on the  $\eta$  electron Fermi surface. **d** and **e** are the same as **b** and **c**, but taken on the  $\delta$  electron Fermi surface. The dashed line in **b**, **c**, **d**, **e** is a guide to the eyes for the variation of the superconducting gap. Hereafter, the momentum location of each spectrum is denoted by either the polar angle  $\theta$  as defined in the insets, or a solid circle on the Fermi surface. All data were taken in the superconducting state at 9 K.

the region with  $k_z = 0.34\pi$ , which is far from Z (see Fig. S3 in supplementary materials for detail). Therefore, gap nodes cannot be accessed by 7 eV photons.

The gap distribution on all the Fermi surfaces of  $\text{BaFe}_2(\text{As}_{0.7}\text{P}_{0.3})_2$  is summarized in Fig. 4a, together with that of  $\text{Ba}_{0.6}\text{K}_{0.4}\text{Fe}_2\text{As}_2$  replicated from Ref.[20] for comparison. The superconducting gaps on the  $\alpha$ ,  $\beta$ ,  $\gamma$ , and  $\delta$  Fermi surfaces vary with  $k_z$  in  $\text{BaFe}_2(\text{As}_{0.7}\text{P}_{0.3})_2$ , while only the gap on  $\alpha$  Fermi surface exhibits significant  $k_z$  dependence in  $\text{Ba}_{0.6}\text{K}_{0.4}\text{Fe}_2\text{As}_2$ . Moreover, the Fermi surface portion affected by the gap nodes in  $\text{BaFe}_2(\text{As}_{0.7}\text{P}_{0.3})_2$  is limited, which explains its relative high  $T_c$ . Figure 4b plots the superconduct-

ing gap of  $\text{BaFe}_2(\text{As}_{0.7}\text{P}_{0.3})_2$  as a function of  $|\cos k_x \cos k_y|$ . There are obvious deviations from the predicted gap function of  $\Delta_0 |\cos k_x \cos k_y|$  based on the  $s^\pm$ -wave pairing symmetry [13–16], which is particularly large for the  $\alpha$  band.

For quantitative analysis, the superconducting gap on each individual Fermi surface of  $\text{BaFe}_2(\text{As}_{0.7}\text{P}_{0.3})_2$  is plotted in Figs. 4c and 4d as functions of  $k_z$ . To account for the  $k_z$  dependence, they are fitted by a phenomenological function:  $\Delta_1 |\cos k_x \cos k_y| + \Delta_2 \cos k_z$ . To achieve a reasonable fit, different  $\Delta_1$  and  $\Delta_2$  have to be exploited for each band although  $\Delta_1$  varies just slightly, indicating the orbital dependency of the gap. However, the gap structure of the  $\alpha$  band cannot be fit-



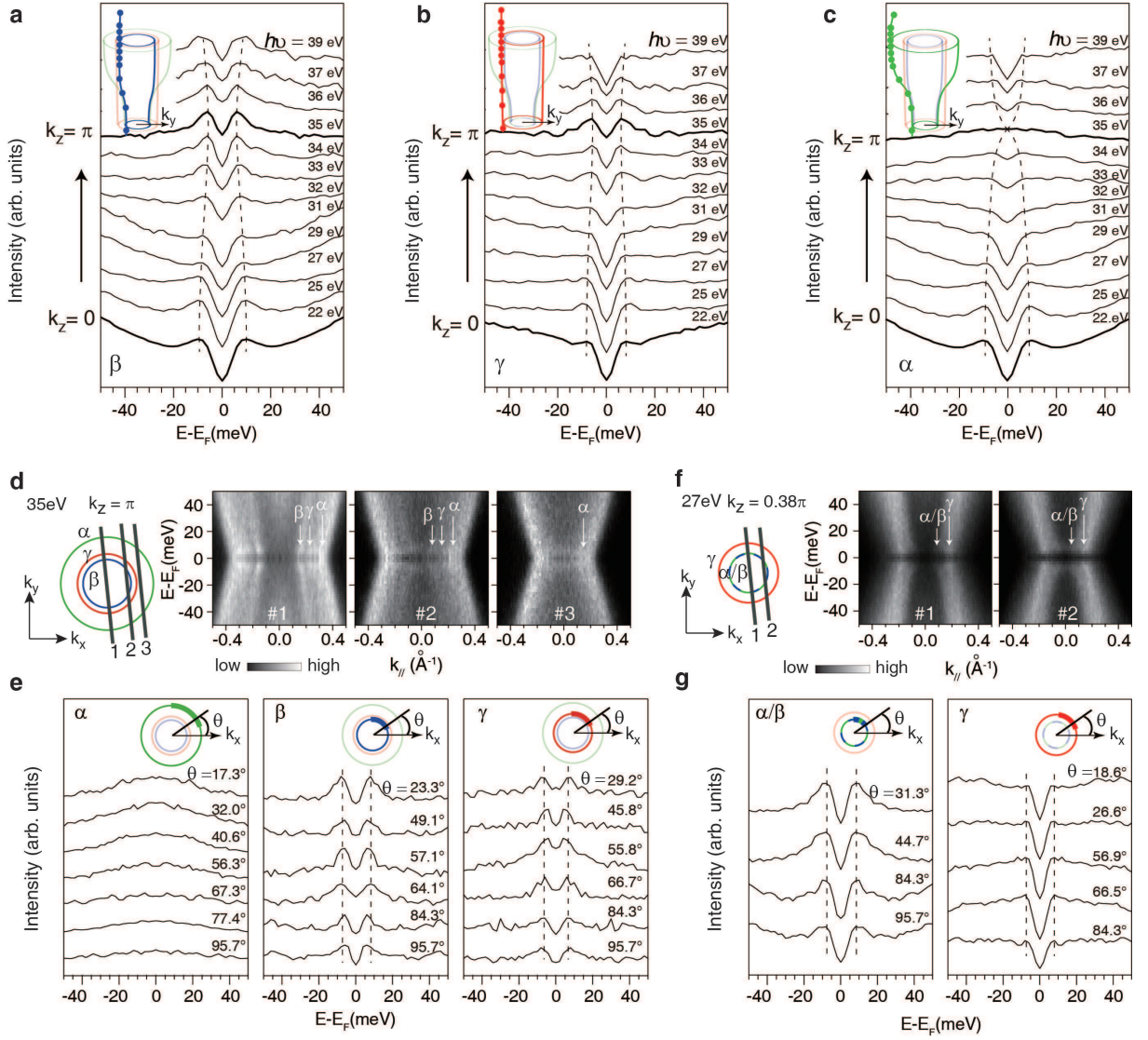


**FIG. 3: The superconducting gap distribution on the hole Fermi surfaces of  $\text{BaFe}_2(\text{As}_{0.7}\text{P}_{0.3})_2$ .** **a-c**,  $k_z$  dependence of the symmetrized spectra measured on the  $\beta$ ,  $\gamma$ , and  $\alpha$  hole Fermi surfaces respectively. The symmetrized spectra near  $k_z = 0$  and  $k_z = \pi$  are shown in thicker lines. The dashed line is a guide to the eyes for the variation of the superconducting gap at different  $k_z$ 's. **d**, The photoemission intensities taken along three momentum cuts and **e**, angular-dependent symmetrized spectra along the  $\alpha$ ,  $\beta$ , and  $\gamma$  hole Fermi surfaces taken with 35 eV photons in the  $k_z = \pi$  plane around Z. **f** and **g** are the same as **d** and **e**, but taken with 27 eV photons in the  $k_z = 0.38\pi$  plane. All data were taken in the superconducting state at 9 K. We note that one can usually distinguish an energy gap if it is bigger than 20% of the resolution in a photoemission experiment, and the energy resolution here with 35 eV photons is 6 meV.

ted well by such a formula (solid line) probably due to strong mixing of another orbital into this band as will be discussed below. As a reference, we plot the  $k_z$  dependence of the gap of the  $\alpha$  band in  $\text{Ba}_{0.6}\text{K}_{0.4}\text{Fe}_2\text{As}_2$  and its fit in Fig. 4e, where the  $k_z$ -contribution to the gap reduction is about 4.2 meV from the  $\Delta_2$  term.

Enforcing a  $\Delta_1 |\cos k_x \cos k_y|$  fit (dashed line) to the superconducting gap of the  $\alpha$  band of  $\text{BaFe}_2(\text{As}_{0.7}\text{P}_{0.3})_2$ , one could estimate the gap with only in-plane momentum contribution. It is about 5 meV around Z (bottom of the dashed line), due to the large radius of the  $\alpha$  Fermi surface in the  $k_z = \pi$  plane. On the other hand, considering the stronger three dimensional

character of the  $\alpha$  band in  $\text{BaFe}_2(\text{As}_{0.7}\text{P}_{0.3})_2$ , it is therefore reasonable to postulate that the  $k_z$ -related reduction of the gap could be even larger than that in  $\text{Ba}_{0.6}\text{K}_{0.4}\text{Fe}_2\text{As}_2$ . As a result, it further reduce the gap by another 5 meV to zero, and create the observed horizontal circular node. That is, the circular nodal gap surrounding Z in  $\text{BaFe}_2(\text{As}_{0.7}\text{P}_{0.3})_2$  could be an “accident” conspired by the relatively small  $\Delta_1$ , the large hole Fermi surface radius around Z, and the sizable  $k_z$ -related gap reduction. It is possible that with increasing  $k_z$ -dependency, the circular node could be reached at a smaller  $k_z$ , and the superconducting order parameter would change sign beyond that  $k_z$ .

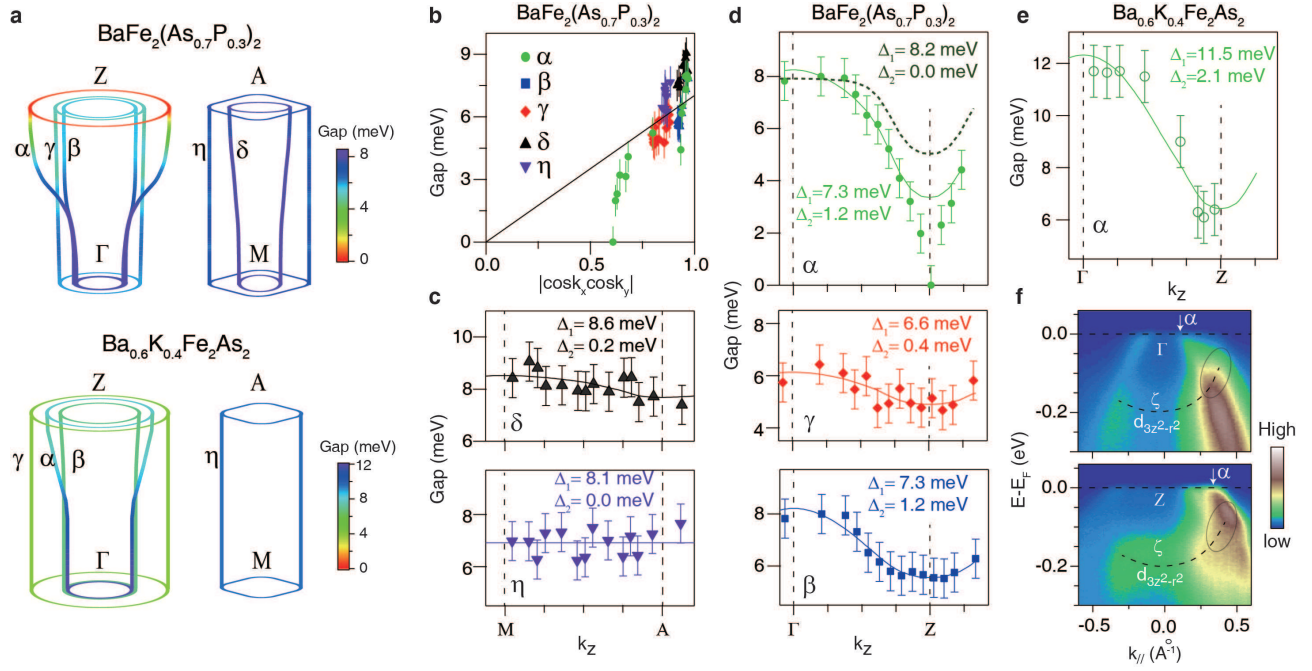


FIG. 4: **Momentum dependency of the superconducting gap.** **a**, False color plots of the gap distribution on the Fermi surfaces of  $\text{BaFe}_2(\text{As}_{0.7}\text{P}_{0.3})_2$  (top) and  $\text{Ba}_{0.6}\text{K}_{0.4}\text{Fe}_2\text{As}_2$  (bottom). **b** The superconducting gap of  $\text{BaFe}_2(\text{As}_{0.7}\text{P}_{0.3})_2$  vs.  $|\cos k_x \cos k_y|$ . **c**, The superconducting gap on the  $\delta$  and  $\eta$  electron Fermi surfaces, and **d** on the  $\alpha$ ,  $\beta$ , and  $\gamma$  hole Fermi surfaces for  $\text{BaFe}_2(\text{As}_{0.7}\text{P}_{0.3})_2$  as functions of  $k_z$ . **e**, The superconducting gap on the  $\alpha$  Fermi surface of  $\text{Ba}_{0.6}\text{K}_{0.4}\text{Fe}_2\text{As}_2$  as a function of  $k_z$ . The error bars are standard deviations of the measured superconducting gaps. **f**, The band structure of  $\text{BaFe}_2(\text{As}_{0.7}\text{P}_{0.3})_2$  near  $\Gamma$  and  $Z$ .

Our findings are consistent with a scenario proposed by Kuroki et al. [27]. They found that with increasing phosphor concentration,  $3d_{3z^2-r^2}$  orbital will be strongly mixed into the  $\alpha$  band near  $Z$ . As a result, the  $s^\pm$  superconducting gap could change sign on the  $\alpha$  Fermi surface near  $Z$ , and thus a nodal circle of superconducting gap emerges on the location where the sign is switched. Furthermore, more phosphor doping will shift the nodal circle from  $Z$  toward  $\Gamma$ . Indeed as illustrated in Fig. 4f and Fig. S6 in the supplementary materials, we do find that the  $\zeta$  band with strong  $d_{3z^2-r^2}$  orbital character comes cross the  $\alpha$  band, and the Fermi crossing of  $\alpha$  is much closer to the top of the  $\zeta$  band near  $Z$  than near  $\Gamma$ . This would induce significant amount of  $d_{3z^2-r^2}$  orbital character into  $\alpha$  near  $E_F$ . This scenario together with our findings provides an possible explanation for the recent intriguing observation that the nodal gap will appear in iron pnictides when the distance between the pnictogen and Fe plane ( $h_{Pn}$ ) is smaller than  $1.33\text{\AA}$ [9]. In

the case of  $\text{BaFe}_2(\text{As}_{1-x}\text{P}_x)_2$ ,  $h_{Pn}$  is reduced by phosphor doping, and consequently, it would cause larger  $k_z$ -dispersion and strong mixing of the  $d_{3z^2-r^2}$  orbital for the  $\alpha$  band as observed, which would create the line node as proposed [27].

To summarize, we have mapped out the detailed superconducting gap distribution of  $\text{BaFe}_2(\text{As}_{0.7}\text{P}_{0.3})_2$ , and found that the line node of superconducting gap is a circle around  $Z$  on the  $\alpha$  Fermi surface, which is likely induced by the strong three dimensional nature of the  $\alpha$  band such as its increasing  $d_{3z^2-r^2}$  orbital character near  $Z$ . Our results rule out the  $d$ -wave pairing symmetry as the cause of the nodal superconductivity, and indicate that  $s^\pm$ -wave pairing symmetry still prevails here. This unifies the seemingly diversified phenomenology of nodal and nodeless superconducting gaps in various iron based superconductors, and provides a discriminator for theories on iron pnictides.

- 
- [1] Ding, H. *et al.* Observation of Fermi-surface-dependent nodeless superconducting gaps in  $\text{Ba}_{0.6}\text{K}_{0.4}\text{Fe}_2\text{As}_2$ . *Europhys. Lett.* **83**, 47001 (2008).
  - [2] Terashima, K. *et al.* Fermi surface nesting induced strong pairing in iron-based superconductors. *Proc. Natl. Acad. Sci. U.S.A.* **106**, 7330 (2009).
  - [3] Zhang, Y. *et al.* Nodeless superconducting gap in  $\text{A}_x\text{Fe}_2\text{Se}_2$  ( $\text{A}=\text{K},\text{Cs}$ ) revealed by angle-resolved photoemission spectroscopy. *Nature Mater.* **10**, 273-277 (2011).
  - [4] Miao, H. *et al.* Isotropic superconducting gaps with enhanced pairing on electron Fermi surfaces in  $\text{FeTe}_{0.55}\text{Se}_{0.45}$ . Preprint at <http://arxiv.org/abs/1107.0985> (2011).
  - [5] Fletcher, J. D. *et al.* Evidence for a nodal-line superconducting state in  $\text{LaFePO}$ . *Phys. Rev. Lett.* **102**, 147001 (2009).
  - [6] Hashimoto, K. *et al.* Line nodes in the energy gap of superconducting  $\text{BaFe}_2(\text{As}_{1-x}\text{P}_x)_2$  single crystals as seen via penetration depth and thermal conductivity. *Phys. Rev. B* **81**, 220501 (2010).

- [7] Yamashita, M. *et al.* Nodal gap structure of  $\text{BaFe}_2(\text{As}_{1-x}\text{P}_x)_2$  determined by the angle resolved thermal conductivity. Preprint available at <http://arxiv.org/abs/1103.0885> (2011).
- [8] Nakai, Y. *et al.*  $^{31}\text{P}$  and  $^{75}\text{As}$  NMR evidence for a residual density of states at zero energy in superconducting  $\text{BaFe}_2(\text{As}_{0.67}\text{P}_{0.33})_2$ . *Phys. Rev. B* **81**, 020503 (2010).
- [9] Hashimoto, K. *et al.* Nodeless vs nodal order parameters in  $\text{LiFeAs}$  and  $\text{LiFeP}$  superconductors. Preprint available at <http://arxiv.org/abs/1107.4505> (2011).
- [10] Dong, J. K. *et al.* Quantum Criticality and Nodal Superconductivity in the FeAs-Based Superconductor  $\text{KFe}_2\text{As}_2$ . *Phys. Rev. Lett.* **104**, 087005 (2010).
- [11] Qiu, X. *et al.* Nodal superconductivity in  $\text{Ba}(\text{Fe}_{1-x}\text{Ru}_x)_2\text{As}_2$  induced by isovalent Ru substitution. Preprint available at <http://arxiv.org/abs/1106.5417> (2011).
- [12] Song, C. L. *et al.* Direct Observation of Nodes and Twofold Symmetry in FeSe Superconductor. *Science* **332**, 1410-1413 (2010).
- [13] Mazin, I. I., Singh, D. J., Johannes, M. D. & Du, M. H. Unconventional Superconductivity with a Sign Reversal in the Order Parameter of  $\text{LaFeAsO}_{1-x}\text{F}_x$ . *Phys. Rev. Lett.* **101**, 057003 (2008).
- [14] Kuroki, K. *et al.* Unconventional Pairing Originating from the Disconnected Fermi Surfaces of Superconducting  $\text{LaFeAsO}_{1-x}\text{F}_x$ . *Phys. Rev. Lett.* **101**, 087004 (2008).
- [15] Seo, K., Bernevig, A. B. & Hu, J. Pairing symmetry in a two-orbital exchange coupling model of oxypnictides. *Phys. Rev. Lett.* **101**, 206404 (2008).
- [16] Hu, J. P. & Ding, H. Local antiferromagnetic exchange and collaborative Fermi surface as key ingredients of high temperature superconductors. Preprint available at <http://arxiv.org/abs/1107.1334> (2011).
- [17] Chen, C. T., Tsuei, C. C., Ketchen, M. B., Ren, Z. A. & Zhao, Z. X. Integer and half-integer flux-quantum transitions in a niobium-iron pnictide loop. *Nature Phys.* **6**, 260-264 (2010).
- [18] Hanaguri, T., Niitaka, S., Kuroki, K. & Takagi, H. Unconventional s-Wave Superconductivity in  $\text{Fe}(\text{Se},\text{Te})$ . *Science* **328**, 474-476 (2010).
- [19] Ye, Z. R. *et al.* Phosphor induced significant hole-doping in ferropnictide superconductor  $\text{BaFe}_2(\text{As}_{1-x}\text{P}_x)_2$ . Preprint available at <http://arxiv.org/abs/1105.5242> (2011).
- [20] Zhang, Y. *et al.* Out-of-plane momentum and symmetry-Dependent energy gap of the pnictide  $\text{Ba}_{0.6}\text{K}_{0.4}\text{Fe}_2\text{As}_2$  superconductor revealed by angle-resolved photoemission spectroscopy. *Phys. Rev. Lett.* **105**, 117003 (2010).
- [21] Yoshida, T. *et al.* Two-dimensional and three-dimensional Fermi surfaces of superconducting  $\text{BaFe}_2(\text{As}_{1-x}\text{P}_x)_2$  and their nesting properties revealed by angle-resolved photoemission spectroscopy. *Phys. Rev. Lett.* **106**, 117001 (2011).
- [22] Kuroki, K., Usui, H., Onari, S., Arita, R. & Aoki, H. Pnictogen height as a possible switch between high- $T_c$  nodeless and low- $T_c$  nodal pairings in the iron-based superconductors. *Phys. Rev. B* **79**, 224511 (2009).
- [23] Wang, F., Zhai, H. & Lee, D.-H. Nodes in the gap function of  $\text{LaFePO}$ , the gap function of the  $\text{Fe}(\text{Se},\text{Te})$  systems, and the STM signature of the  $s_{\pm}$  pairing. *Phys. Rev. B* **81**, 184512 (2010).
- [24] Thomale, R., Platt, C., Hanke, W. & Bernevig, B. A. Why some Iron-based superconductors are nodal while others are nodeless. *Phys. Rev. Lett.* **106**, 187003 (2011).
- [25] Vildosola, V. *et al.* Bandwidth and Fermi surface of iron oxypnictides: Covalency and sensitivity to structural changes. *Phys. Rev. B* **78**, 064518 (2008).
- [26] Shimojima, T. *et al.* Orbital-independent superconducting gaps in iron-pnictides, *Science* **332**, 564-567 (2011).
- [27] Suzuki, K., Usui, H. & Kuroki, K. Possible three dimensional nodes in the  $s_{\pm}$  superconducting gap of  $\text{BaFe}_2(\text{As}_{1-x}\text{P}_x)_2$ . *J. Phys. Soc. Jpn.* **80**, 013710 (2011).

**Methods:** High quality  $\text{BaFe}_{2.1}(\text{As}_{0.7}\text{P}_{0.3})_{1.9}$  single crystals with superconducting transition temperature  $T_c = 30$  K were synthesized through flux-free crucible growth. Shiny platelet crystals as large as  $2 \times 2 \times 0.05 \text{ mm}^3$  were obtained with residual resistivity ratio of about 10 (see supplementary information for details). The compositions were measured by an energy dispersive X-ray (EDX) analysis. Data were taken at the Beamline 5-4 of Stanford Synchrotron Radiation Lightsource (SSRL). All the data were taken with Scienta electron analyzers, the overall energy resolution was 5-8 meV depending on the photon energy, and the angular resolution was 0.3 degree. The samples were cleaved *in situ*, and measured under ultra-high-vacuum of  $5 \times 10^{-11} \text{ torr}$ .

**Acknowledgement:** The authors thank Prof. J. P. Hu, and Prof. X. H. Chen for fruitful discussions, and thank Dr. D.H. Lu for the experimental assistance at SSRL. This work is supported in part by the National Science Foundation of China, Ministry of Education of China, Science and Technology Committee of Shanghai Municipal, and National Basic Research Program of China (973 Program) under the grant Nos. 2011CB921802 and 2011CBA00112. SSRL is operated by the US DOE, Office of Basic Energy Science, Divisions of Chemical Sciences and Material Sciences.

**Supplementary information for:**  
**Nodal superconducting gap structure in ferropnictide superconductor**  
 **$\text{BaFe}_2(\text{As}_{0.7}\text{P}_{0.3})_2$**

Y. Zhang,<sup>1</sup> Z. R. Ye,<sup>1</sup> Q. Q. Ge,<sup>1</sup> F. Chen,<sup>1</sup> Juan Jiang,<sup>1</sup> M. Xu,<sup>1</sup> B. P. Xie,<sup>1</sup> and D. L. Feng<sup>1,\*</sup>

*<sup>1</sup>State Key Laboratory of Surface Physics, Department of Physics,  
and Advanced Materials Laboratory, Fudan University,  
Shanghai 200433, People's Republic of China*

---

\*Electronic address: dlfeng@fudan.edu.cn

## I. SAMPLE DESCRIPTION

High quality  $\text{BaFe}_2(\text{As}_{1-x}\text{P}_x)_2$  ( $x = 0.30$ ) single crystals were synthesized with a flux-free method. Ba, FeAs and FeP were mixed with the nominal compositions, loaded into an alumina tube, and then sealed into a stainless steel crucible under the Ar atmosphere. The entire assembly was heated to 1673 K and kept for 12 h or longer, and then slowly cooled down to 1173 K at the rate of 4 K/h before shutting off the power. Shining platelet crystals as large as  $2 \times 2 \times 0.05 \text{ mm}^3$  were obtained as shown in the inset of Fig. S1a. The resistivity of  $\text{BaFe}_2(\text{As}_{0.7}\text{P}_{0.3})_2$  single crystal shows a sharp superconducting transition at 30 K, with the transition width less than 0.5 K (Fig. S1a). The room temperature-to-residual resistivity ratio is  $\approx 10.4$ , indicating minimal disorder and impurity of the single crystal. The magnetic susceptibility as a function of temperature was measured in a 20 Oe magnetic field (Fig. S1b). A sharp drop in the zero field cooling (ZFC) susceptibility, indicating the onset of superconductivity, appears at 30 K, which is consistent with the zero-resistivity temperature in Fig. S1a. The ZFC and field cooling (FC) curves indicate a bulk superconductivity nature and high quality of the crystals.

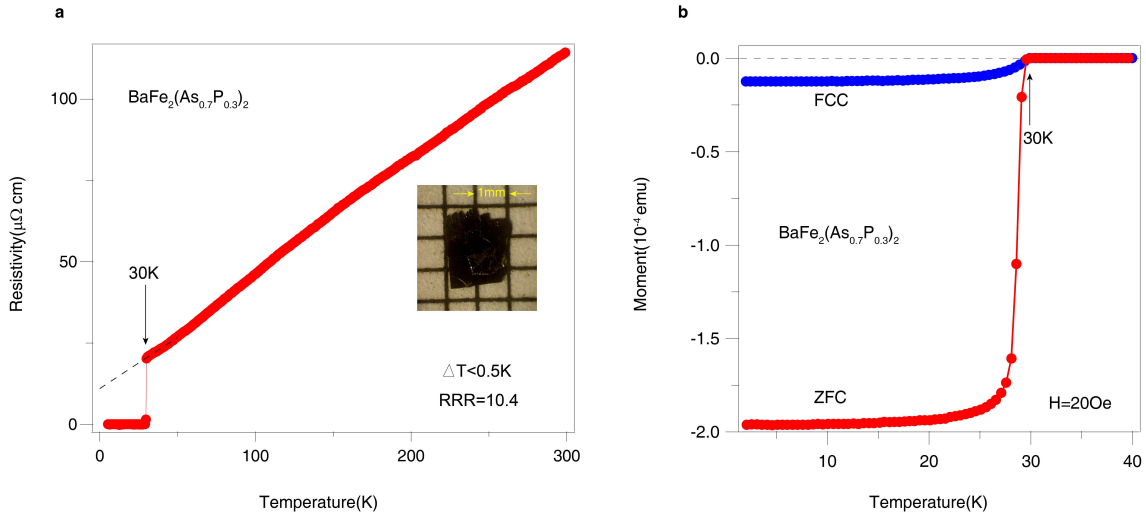


FIG. S1: **Resistivity and magnetic susceptibility of  $\text{BaFe}_2(\text{As}_{0.7}\text{P}_{0.3})_2$ .** **a**, Temperature dependence of resistivity. The inset is the photograph of a  $\text{BaFe}_2(\text{As}_{0.7}\text{P}_{0.3})_2$  single crystal. **b**, Temperature dependence of magnetic susceptibility in a 20 Oe magnetic field.



## II. DETERMINATION OF THE SUPERCONDUCTING GAP

To determine the gap size, we fit the symmetrized spectra or energy distribution curves (EDCs) with a simple empirical spectral function described in Ref. 1. The self-energy at the normal state Fermi crossing ( $k_F$ ) in the superconducting state may be expressed as

$$\Sigma(k_F, \omega) = -i\Gamma + \frac{\Delta^2}{\omega}$$

where  $\Gamma$  is the inverse life time of the quasi-particle related to the width of the spectrum and  $\Delta$  represents the gap at  $k_F$ . The spectral function is calculated according to

$$A(k_F, \omega) = -\frac{1}{\pi} \text{Im} \frac{1}{\omega - \Sigma(k_F, \omega)}$$

The spectral function was convoluted with a Gaussian representing the instrumental resolution. The spectral background is fitted by a fourth order polynomial. We note that some variations of the smooth background has minimal effect on the fitted superconducting gap size. The gap is most determined by the peak position near the Fermi energy ( $E_F$ ) in the symmetrized EDCs. Due to the broad line shape and small spectral weight of the superconducting peak here, the superconducting gap determined through the fitting procedure is usually about 1 meV smaller than the gap value determined directly from the superconducting peak position. As an example, the fit of the data in the left panel of Fig. 1c are shown in Fig. S2, which gives the gap value of the  $\alpha/\beta$  band as a function of temperature.

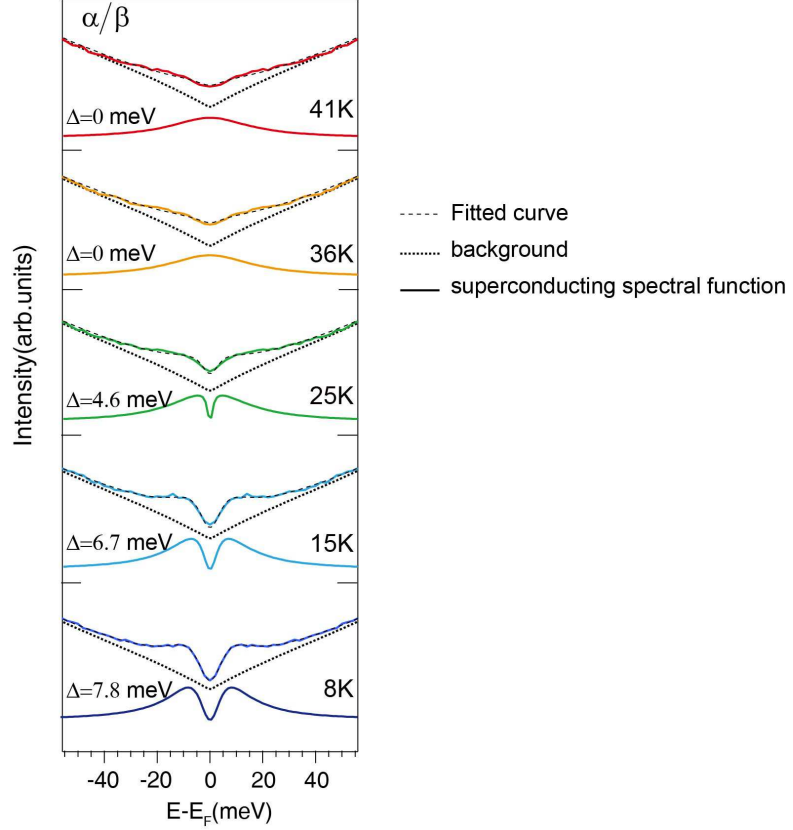


FIG. S2: **An empirical fit for retrieving the superconducting gap value of  $\text{BaFe}_2(\text{As}_{0.7}\text{P}_{0.3})_2$ .** The symmetrized spectra measured at different temperatures are fitted by the empirical spectral function. Data were taken at a Fermi crossing of the  $\alpha/\beta$  Fermi surface near  $\Gamma$  (also shown in Fig. 3c in the main text). The fitted curve, background, and superconducting spectral function are shown in black dashed line, dot line, and solid line respectively.

### III. DETERMINATION OF $k_z$

In angle resolved photoemission spectroscopy, a specific out-of-plane momentum  $k_z$  can be accessed with a particular photon energy according to

$$k_z = \sqrt{\frac{2m}{\hbar^2}[(h\nu - \Phi)\cos^2\theta + V_0]}$$

where  $h\nu$  is the photon energy,  $\Phi$  is the work function, and  $V_0$  is the inner potential of the sample [2]. To determine  $V_0$ , we plot the photon energy dependence of the momentum distribution curves (MDCs) near  $E_F$  along high symmetry directions in the Brillouin zone in Fig. S3. The position of the MDCs represents the band dispersion as a function of  $k_z$ , and one could search for the

symmetry in the band dispersion enforced by the Brillouin boundary. For example in Fig. S3a, the peak position of  $\alpha$  is outmost at 35 eV, representing the largest Fermi surface at the Z point. Through trial and error, we finally pick the inner potential of 14.5 eV to calculate the  $k_z$  in order to achieve best agreement with all our photon energy dependent data in Fig. S3. The determination of  $k_z$ 's for different photon energies are shown in Fig. S3c, where the cuts taken with 22, 35, 27, and 18 eV photons sample momentum regions near  $\Gamma$ , Z, M, and A, respectively. Based on our  $V_0$ , the  $k_z$  is about  $0.34\pi$  for the cut taken with 7 eV photons. Note that, the  $k_z$  is folded into the upper half of the first Brillouin zone for simplicity in the main text.

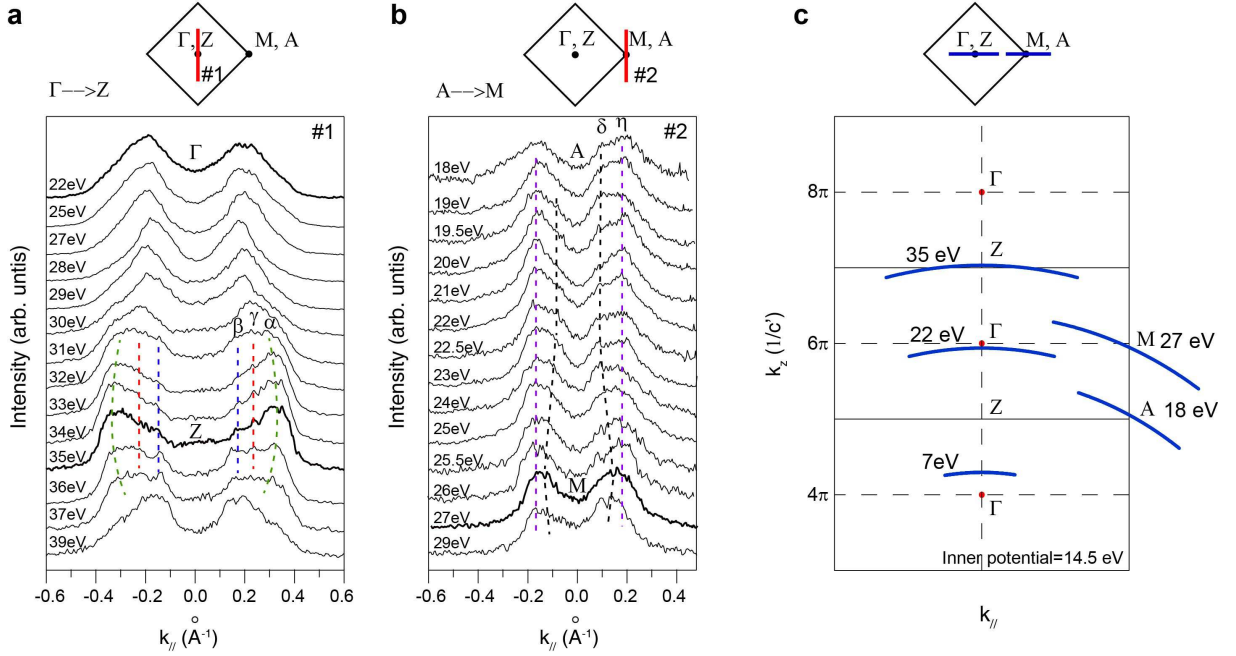


FIG. S3: **Photon energy dependent data of  $\text{BaFe}_2(\text{As}_{0.7}\text{P}_{0.3})_2$ .** **a**, The photon energy dependent momentum distribution curves (MDCs) near  $E_F$  taken along cut #1. The peak positions of the MDCs represent the Fermi crossings of the hole Fermi surfaces near the zone center. **b** is the same as **a** but taken along cut #2, where the peak positions of the MDCs represent the Fermi crossings of the electron Fermi surfaces near the zone corner. **c**, The illustration of the  $k_z$  calculation for the cuts taken with 22, 35, 27, 18, and 7 eV photons.

#### IV. SYMMETRIZED EDCS ON THE ELECTRON AND HOLE FERMİ SURFACES

In addition to the data presented in Fig.2, Fig. S4 present more superconducting gap measurement on the electron Fermi surfaces of  $\text{BaFe}_2(\text{As}_{0.7}\text{P}_{0.3})_2$  in the  $k_z = 0.2\pi, 0.34\pi, 0.54\pi, 0.64\pi, 0.8\pi$  planes. The superconducting gap is finite in every symmetrized EDC. The extensive survey gives compelling evidence on the absence of line node on the two electron Fermi surfaces in  $\text{BaFe}_2(\text{As}_{0.7}\text{P}_{0.3})_2$ .

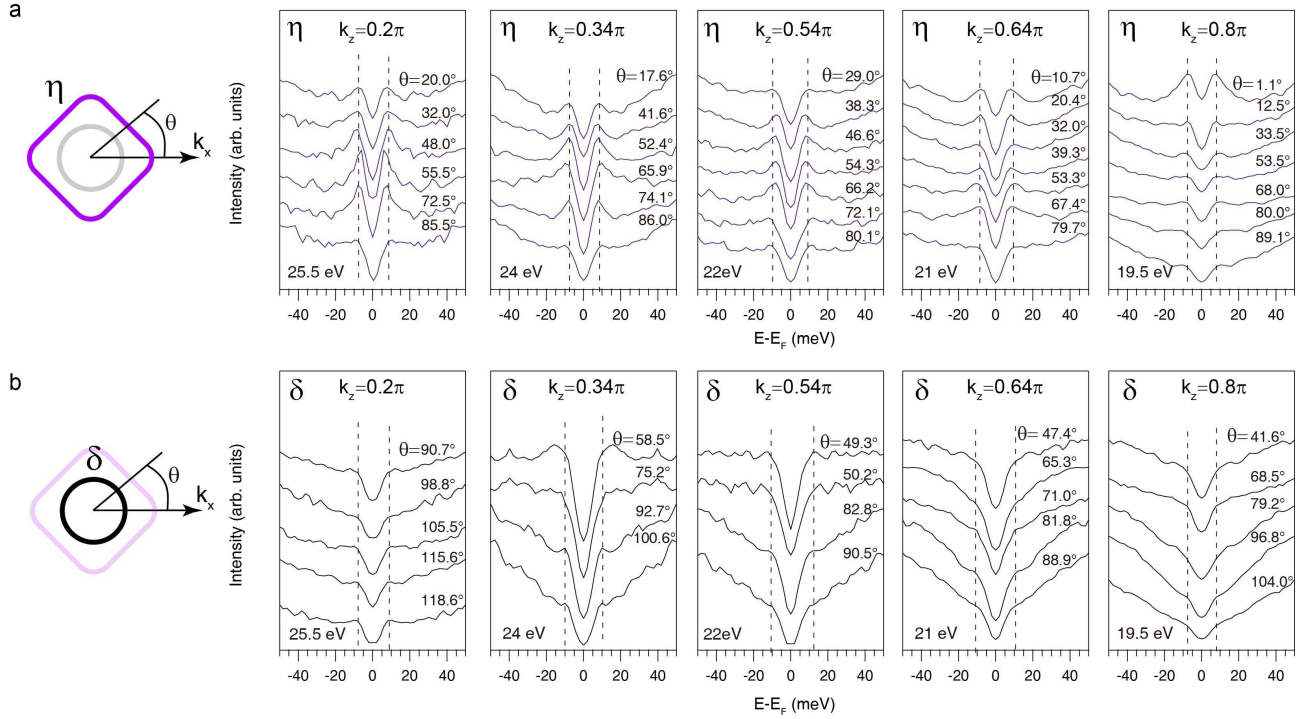


FIG. S4: **The symmetrized EDCs on the electron Fermi surfaces.** **a**, The angular-dependent symmetrized EDCs measured on the  $\eta$  electron Fermi surfaces with different photon energies. **b**, The angular-dependent symmetrized EDCs measured on the  $\delta$  electron Fermi surfaces with different photon energies.

In addition to the data presented in Fig. 3g, Fig. S5 present more superconducting gap measurement on the hole Fermi surfaces of  $\text{BaFe}_2(\text{As}_{0.7}\text{P}_{0.3})_2$  in the  $k_z = 0$  plane. The gap distribution is isotropic and finite here.

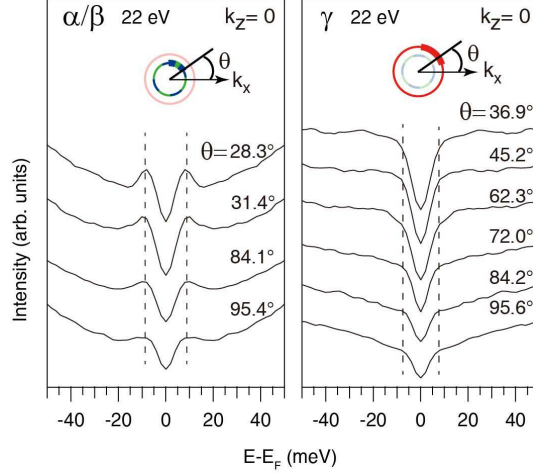


FIG. S5: **The symmetrized EDCs on the hole Fermi surfaces.** The angular-dependent symmetrized EDCs measured on the hole Fermi surfaces with 22 eV photons near the  $\Gamma$  point.

## V. STRONGER MIXING OF $d_{z^2}$ ORBITAL INTO THE $\alpha$ BAND NEAR Z

Previous experimental and theoretical studies on the electronic structure of iron-based superconductors report that the  $d_{3z^2-r^2}$  orbital form two bands that are below  $E_F$  [3, 4]. In  $\text{BaFe}_2(\text{As}_{0.7}\text{P}_{0.3})_2$ , the  $\zeta$  band with  $d_{3z^2-r^2}$  orbital is at about 200 meV below  $E_F$  near the  $\Gamma$  point as shown in Figs. S6a. Near  $\Gamma$ , one could trace the MDCs peaks correspond to  $\zeta$  disperse vertically towards  $E_F$  as marked by the solid squares in Fig. S6b at about  $k_{\parallel} \approx 0.3 \text{ \AA}^{-1}$ . This indicates these are just the residual of the broad  $\zeta$  feature below  $E_F$ . In other words, although the  $\zeta$  band does not cross  $E_F$ , it could contribute finite spectral weight even at  $E_F$ . The  $\alpha$  band crosses  $E_F$  at  $0.1 \text{ \AA}^{-1}$  near  $\Gamma$ , and at  $0.33 \text{ \AA}^{-1}$  near Z (Figs. S6a and S6c). In the MDCs taken around Z shown in Fig. S6d, the features of  $\alpha$  and those of  $\zeta$  are too close to be distinguished. Thus, the  $d_{3z^2-r^2}$  orbital character in the  $\zeta$  band should mix rather strongly with the  $\alpha$  band near  $E_F$  around the Z point [5].



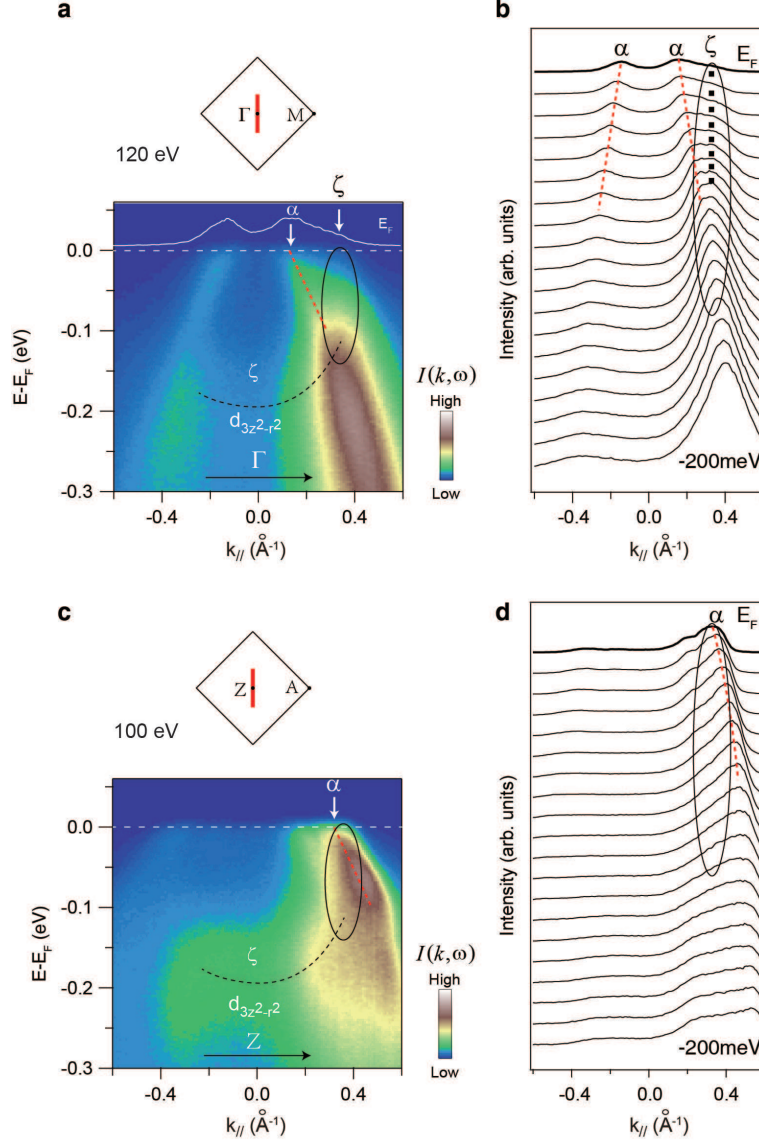


FIG. S6: **The photoemission data of  $\text{BaFe}_2(\text{As}_{0.7}\text{P}_{0.3})_2$  near  $E_F$  taken in the  $p$  polarization [5].** **a**, The photoemission intensity taken with 120 eV photons around  $\Gamma$  in the  $p$  polarization. Dashed lines are band dispersions. The black ellipse indicates the spectral weight of the  $\zeta$  band. The inset in **a** is the MDC at  $E_F$ . **b**, The MDCs of the data in **a**. **c**, The photoemission intensity taken with 100 eV photons around  $Z$  in the  $p$  polarization. **d** The MDCs of the data in **c**.

- 
- [1] Norman, M. R., Randeria, M., Ding, H. & Campuzano, J. C. Phenomenology of the low-energy spectral function in high- $T_c$  superconductors. *Phys. Rev. B* **57**, R11093 (1998).

- [2] Hufner, S., Photoelectron Spectroscopy. *Springer* (1995).
- [3] Zhang, Y. *et al.* Orbital characters of bands in the iron-based superconductor  $\text{BaFe}_{1.85}\text{Co}_{0.15}\text{As}_2$ . *Phys. Rev. B* **83**, 054510 (2011).
- [4] Graser, S., Maier, T. A., Hirschfeld, P. J. & Scalapino, D. J. Near-degeneracy of several pairing channels in multiorbital models for the Fe-pnictides. *New J. Phys.* **11**, 025016 (2009).
- [5] Ye, Z. R. *et al.* Phosphor induced significant hole-doping in ferropnictide superconductor  $\text{BaFe}_2(\text{As}_{1-x}\text{P}_x)_2$ . Preprint at <http://arxiv.org/abs/1105.5242>.